DELFT UNIVERSITY OF TECHNOLOGY

REPORT 13-08

3D Nonlinear Transient Field-Circuit Modeling of Inductive Fault Current Limiters

D. Cvoric, D. Lahaye, S. W. H. de Haan and J. A. Ferreira

ISSN 1389-6520

Reports of the Department of Applied Mathematical Analysis

Delft 2013

INTERNATIONAL JOURNAL OF NUMERICAL MODELLING: ELECTRONIC NETWORKS, DEVICES AND FIELDS
Int. J. Numer. Model. 0000; **00**:1–7
Published online in Wiley InterScience (www.interscience.wiley.com). DOI: 10.1002/jnm

3D Nonlinear Transient Field-Circuit Modeling of Inductive Fault Current Limiters

D. Cvoric*, D. Lahaye**, S. W. H. de Haan* and J. A. Ferreira*
* Electrical Power Processing Unit, ** Numerical Analysis Unit
Delft University of Technology, The Netherlands
{d.cvoric,d.j.p.lahaye}@tudelft.nl

SUMMARY

Due to increasing levels of fault currents, Fault Current Limiters (FCLs) are expected to play an important role in the protection of future power grids. Inductive saturable FCLs are particularly interesting due to their inherent reaction on the fault. Many different configurations have been proposed in literature. Being difficult or impossible to create accurate analytical models of some FCL configurations, the development of Finite Element (FE) models for inductive FCLs is required. This paper presents a 3D nonlinear transient FE modeling technique applied to two inductive FCLs, namely so-called open-core and three-leg single-core FCLs. The models have been validated by comparing simulation results with lab measurements. Results show excellent agreement. The models constitute a valuable tool for design, optimization and verification of inductive FCLs. Copyright © 0000 John Wiley & Sons, Ltd.

Received ...

KEY WORDS: Fault Current Limiters, Finite Element Modeling, Nonlinear Magnetics, Power System Protection

1. INTRODUCTION

Fault Current Limiters (FCLs) are expected to play an important role in the protection of future power grids. They are capable of preventing the fault currents from reaching too high levels and, therefore, reducing the mechanical and thermal stress of all power system components.

FCLs can be classified on passive, solid-state and hybrid FCLs [1]. Passive FCLs are particularly interesting due to inherent reaction on the fault. Inductive FCLs based on the core saturation belongs to the class of the passive FCLs. They comprise magnetic cores and windings. Different configurations of inductive FCL are proposed in literature [1]-[4]. It is difficult, or in some cases impossible, to derive accurate analytical models of FCL designs.

The goal of this paper is to introduce a 3D nonlinear transient Finite Element (FE) modeling technique applied to inductive core-saturable FCLs. The technique constitutes a valuable tool for verification and optimization of the inductive FCL. The operation of the designed FCL can be verified precisely, with the possibility to vary all design parameters. Experiments with both the three-leg [2] and open-core [3] FCL configurations were performed in the lab in order to provide reference data for the verification of the models. 3D simulation results for the limited current show excellent agreement with measurements.

2. PRINCIPLE OF OPERATION OF INDUCTIVE FCLS

Inductive FCLs behave as variable inductors, owing to the ac winding's inductance dependency on the relative permeability of the core, i.e. $L_{FCL} = L_{FCL}(\mu)$. The ac winding of FCL is connected in series to the line; its impedance during normal operation of the system is very low and does not influence the normal current. To achieve this, additional dc winding is wound on the core and connected to a dc current source. It drives the core deep to saturation, which results in a low value of the core permeability (i.e. winding inductance). After a fault inception, the rising fault current flows through the ac winding and takes the core out of saturation. As a result, the impedance of the ac winding increases and restrains the fault current.

How this principle is put into practise is shown in the following two examples.

2.1. Open-Core FCL Configuration

The open-core FCL, shown in Fig.1(a), consists of a single core with one ac and one dc winding per-phase [3]. The dc winding is connected to a current source and saturates the core. The ac winding is connected in series with a line. During the normal regime, the core remains saturated and the inductance of the ac winding is very low. After a fault inception, left and right legs of the core are alternately de-saturated by the fault current, imposing large impedance into the line and restraining the fault. Further details on this topology can be found in [3].

2.2. Three-Leg Single-Core FCL Configuration

The three-leg single-core FCL, shown in Fig.1(b) has one core per phase [2]. Each outer leg contains one ac and one dc winding. The dc windings are connected in series and provide circular dc flux flow, saturating the outer legs of the core. The ac flux closes its path through the left (in another half cycle right leg) and the middle leg of the core. The middle leg provides a shunt path for the ac flux. Upon a fault inception, the outer legs are alternately de-saturated from one half-cycle to another, resulting in increased FCL impedance. Further details on this FCL topology can be found in [2].

3. LAB EXPERIMENTS

To provide reference data for the models developed, experiments are done in the lab. The experimental circuit consists of a power supply, load resistor, dc current source and triggering circuit. A fault is initiated using a triggering circuit and electromechanical relay. Table I gives the parameters of the electrical circuit.

Table I. Parameters of the Electrical Circuit

Parameter	Value
Supply voltage V_e [V_p]	28.2
Nominal line current I_{nom} [A_p]	5
Fault current I_{fault} [A_p]	22
dc current I_{dc} [A]	10
Resistance R_{load} [Ω]	4.5

The open-core lab model is presented in Fig.1(a). As stated earlier, it has one ac and one dc winding. The three-leg FCL is presented in Fig.1(b). Both outer legs comprise one ac and one dc winding. A gap is placed in the middle leg. Laminated silicon-steel cores are used for the experiments. Table II gives the FCL parameters.

DOI: 10.1002/jnm

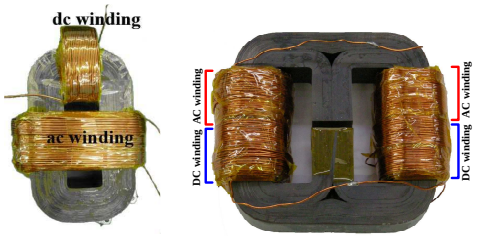

(a) Open-core FCL (b) Three-leg core FCL

Figure 1. FCLs used in the experiment

Table II. Parameters of the FCL prototypes

FCL parameter	Three-leg	Open-core
Core cross-section S_{cr} $[cm^2]$	6.5	12.625
Core width c_w [cm]	12.8	7.5
Core height c_h [cm]	13	12.6
Core depth c_h [cm]	2.5	5.05
Window width w_w [cm]	2.5	2.5
Window height w_h [cm]	7.8	7.8
Number of dc turns N_{dc} [turn]	170	250
Number of ac turns N_{ac} [turn]	170	200
Resistance of ac winding R_{ac} [Ω]	1.3	1.3
DC winding height dc_h [cm]	3	1.6
DC winding width dc_w [cm]	2	2.2
AC winding height ac_h [cm]	3	3.7
AC winding width ac_w [cm]	2	1.3

4. CIRCUIT MODEL

The current I in an RL-circuit with variable inductance satisfies the following circuit equation

$$\frac{d}{dt}(L\,I) + RI = V_e(t)\,, \tag{1}$$

stating that at all times the sum of the induced V_{ind} and resistive V_{res} voltage is equal to the externally supplied one. If therefore the amplitude of the applied voltage is to stay constant, any drop in the resistive voltage must be compensated by an increase in its induced counterpart. Denoting the core cross-section and number of turns by S_{cr} and N_w, respectively, the induced voltage can be expressed by the law of Faraday-Lenz as the time derivative magnetic flux through S_{cr}

$$V_{\text{ind}} = -\frac{d\psi(t)}{dt} \text{ where } \psi(t) = N_w \int_{S_{cr}} \mathbf{B}(\mathbf{x}, t) \cdot d\mathbf{S}\,. \tag{2}$$

In the application considered, the impedance of the ac coil is time-dependent through the permeability μ of the ferromagnetic core. The equation for the current in the ac coil can be solved by assuming a lumped parameter approximations for L as e.g. in [1]

$$L(t) = \mu(t)\, N_w^2 \frac{S_{cr}}{l_{\text{path}}}\,, \tag{3}$$

where l_{path} denotes the average length of the flux path. If μ can be computed from ψ using the B-H curve, then Equation (1) is equivalent to the following non-linear ordinary differential equation for

DOI: 10.1002/jnm

ψ

$$\frac{d}{dt}\psi + \frac{R}{L(\psi)}\psi = V_e(t)\,. \tag{4}$$

Having solved this equation for $\psi(t)$, $I(t)$ can be computed in a post-processing stage.

The shortcomings of the presented circuit model is that fringing and leakage effects of the flux are not accounted for in expressions like Equation (3). It is furthermore not clear how to define the cross-section S_{cr} in case that the coil consists of multiply layers of windings. This motivates the development of a field-circuit coupled model in the next section.

5. FIELD-CIRCUIT COUPLED MODEL

The field-circuit coupled model consists of a partial differential equation for the magnetic field in the FCL, coupled with an ordinary differential equation for the current in the ac coil. Both are coupled by the magnetically induced voltage in the AC coil. We introduce the so-called coil winding function $\mathbf{z}(\mathbf{x})$ [7]-[8], in such a way that the applied current density in the coils can be written as

$$\mathbf{J}_e(\mathbf{x}, t) = \frac{N_w\, I(t)}{S_{ac}}\, \mathbf{z}(\mathbf{x})\,, \tag{5}$$

where S_{ac} denotes the cross-section of the ac coil. The magnetic field equation in the magnetic vector potential $\mathbf{A}$ can then be written as [5]

$$\sigma \frac{\partial \mathbf{A}}{\partial t} + \nabla \times \mu_0^{-1}\mu_r^{-1}\,(\nabla \times \mathbf{A}) = \mathbf{J}_e\,. \tag{6}$$

This system of partial differential equations has to be coupled with Equation (1), where instead of (2) the induced voltage is computed by a homogenization procedure over the turns in the winding resulting in the following integral of the components of the electrical field $\mathbf{E}$ in the direction of the winding over the volume of the ac coil

$$V_{ind} = \frac{N_w}{S_{ac}} \int_{\Omega_{ac}} \mathbf{E} \cdot \mathbf{z}\, d\Omega\,, \tag{7}$$

avoiding the ambiguity in the definition the surface S_{cr}. In case of the three-leg configuration discussed in Subsection 2.2, the induced voltage consists of two contributions corresponding to the separate ac coils. The fault inception is simulated by allowing the Ohmic resistance $R(t)$ in (1) to drop from $R_{load} + R_{ac}$ to R_{ac} given in Table I and Table II at a particular time instance. We specify a non-linear B-H-curve for magnetic relative permeability μ_r in the core and set the electric conductivity σ to zero in both the coils and the core, neglecting induced currents. Neglecting σ throughout the computational domain results the spatially discrete magnetic field operator with a non-trivial null-space. To avoid that numerical iterative procedures such as Newton and time-integration methods to build up components in this non-trivial null-space, we take the Coulomb gauging condition into account and solve for both the vector potential and a gauging field.

We implemented our model in Comsol Multiphysics 3.5 [6] which is a general purpose software environment for the finite element resolution of PDEs akin to MATLAB for numerical linear algebra. In describing our implementation we will employ some nomenclature inherent to the package. For the magnetic field equation (6) including gauging, we employed the predefined application mode for quasi-static magnetic fields. In this application mode the induced voltage can be computed by introducing an integration coupling variable, integrating the electrical field over the subdomain of the ac coil(s). This approach allows to monitor the induced voltage and to compare the result of (2) and (7). The induced voltage is inserted in the circuit equation that is implemented as an ordinary differential equation. A strong coupling between the field and circuit equation is made.

The model is discritized in space using second order $H(curl)$ conforming edge elements for the vector potential and second order nodal for the gauge field on an unstructured mesh of tetrahedra.

Prepared using jnmauth.cls
DOI: 10.1002/jnm

The resulting spatially discrete model is integrated in time using a BDF scheme from DASPK [10] with an adaptively chosen time stepping scheme. The accuracy of this procedure is governed by specifying absolute and relative tolerances on vector potential and gauging field. The adaptive time stepping results in smaller time steps close to the instance when the fault occurs. The system of linear equations arising at each Newton step within each time step is solved using the sparse direct solver PARDISO [11]. The presence of the circuit equation (1) prevents the straightforward deployment of fast multigrid solution techniques [9]. Convergence of the Newton process at the initial time step is obtained by providing a good initial guess. Such a guess is obtained by solving a separate application model in which only the dc coils are excited. Convergence of the Newton process at subsequent time steps required us to overrule the Comsol Multiphyics default values for the evaluation of the Jacobian and the maximum number of Newton iterations.

6. VALIDATION OF THE NUMERICAL MODEL

To validate the developed FEM models, the computed results are compared with the experimental one for both FCL topologies. The non-linear B-H curve, used in simulations, is given in Fig.2. It is obtained by measuring the B-H curve of the used silicon-steel cores. Each simulation is ran from

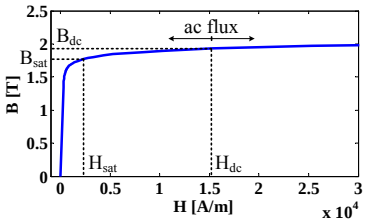

Figure 2. BH curve used in the simulations

t_{start}=0s to t_{end}=0.07s, having a fault incepted at t_{fault}=0.035s as shown in Fig.3(a). As a result, the left and right legs of the open-core are driven alternately out of saturation by rising fault current, see Fig.3(b), resulting further in the increased induced voltage across the ac winding (see Fig.3(a)) and restrained fault current.

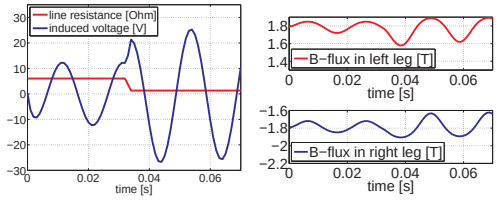

(a) Resistance and Voltage (b) Core leg flux

Figure 3. Simulated line resistance drop, induced voltage and core leg flux in open core FCL.

Fig.4(a) and Fig.4(b) give comparison of the results for the three-leg FCL configuration, for the cases that the gap length is 0mm and 3.5mm, respectively. The models give very accurate results. The current waveforms for open-core FCL are plotted in Fig.5. Again, the graph shows an excellent match. This confirms that the 3D model can indeed be used to predict the behavior of the FCL.

Plots of relative permeability in the FCL core, given in Fig.6, demonstrate the operation principle of both FCL configurations. The right leg of the open-core FCL is saturated at $t = 0.05$s while the left leg is driven out of saturation (see Fig.6(a)), resulting in higher permeability value and increased FCL limiting impedance. The three-leg FCL operates in the similar way. The left outer leg is desaturated, contributing to the enlarged FCL impedance, while the right outer leg is driven deeper to saturation, see Fig.6(b). The given plots are valid for one half-cycle.

DOI: 10.1002/jnm

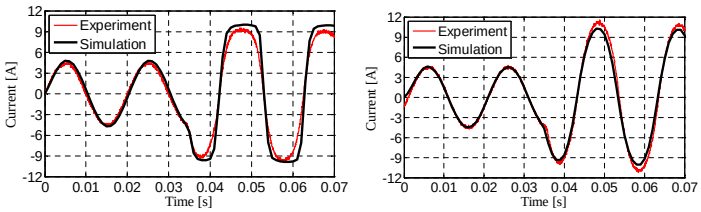

(a) Three-legs FCL without gap (config 1)

(b) Three-legs FCL with 3.5mm gap (config 2)

Figure 4. 3D simulation and experimental current waveforms

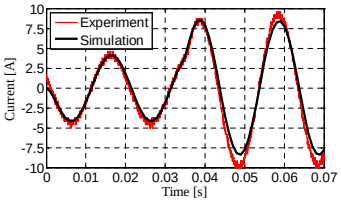

Figure 5. 3D simulation and experimental current waveforms for open-core FCL (config 3)

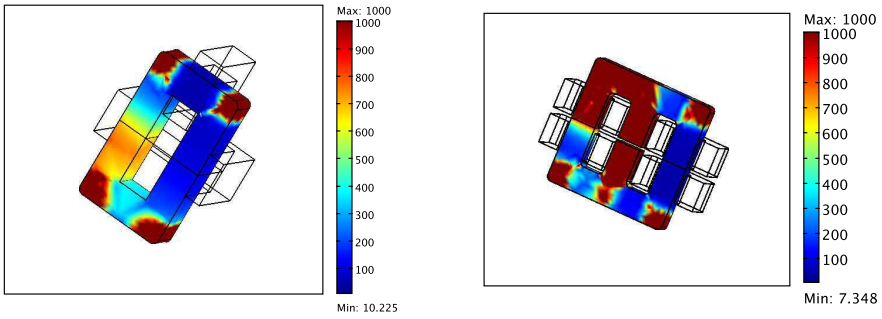

(a) Open-core FCL

(b) Three-leg FCL

Figure 6. Snap shot of relative permeability in the core at $t = 0.05$ s.

Table III. Computational cost of the three configurations considered.

	config 1	config 2	config 3
DOFS	50577	51748	16672
Number of time steps	3002	312	421
Number of Newton steps	1264	709	1147
Simulation time [s]	52581	12248	4358

We performed a mesh convergence study which shows that the instantaneous value of the currents plotted in Fig. 4 and Fig. 5 converge to a limit value as the mesh width converges to zero. In Table III we give the CPU time required to solve the three configurations considered (labeled as config 1, config 2 and config 3) on an Intel 4 3.4 GHz 4 GB RAM workstation. This time is directly related to the number of degrees of freedom, the number of time steps and the total number of Newton steps. In Table III we choose a sufficiently fine mesh according to our convergence study. The table shows that the configuration without gap (config 1) requires more computational effort to solve than its

Prepared using jnmauth.cls
DOI: 10.1002/jnm

counterpart with 3.5mm gap (config 2). Explaining this phenomenon in detail is a matter of further research.

7. CONCLUSION

We presented a three-dimensional non-linear transient field-circuit coupled model that allows to accurately predict the current limiting behavior of inductive FCLs. The model has been treated numerically by a finite element technique. Simulation results for the limited current for two configurations show an excellent match with experimental data. The models presented constitutes a valuable tool for design, optimization and verification of inductive FCLs.

ACKNOWLEDGEMENT

This project is partially funded from the Energy Research Program (EOS) by the Ministry of Economic Affairs.

The authors graterfully acknowledge the valuable feedback provided by Prof. Herbert De Gersem and by the Comsol Multiphysics support team.

REFERENCES

1. D. Cvoric, S.W.H. de Haan and J.A. Ferreira, *Improved Configuration of the Inductive Core-Saturation Fault Current Limiter with the Magnetic Decoupling*, IEEE Industry Applications Society (IAS) Annual Meeting 2008, pp. 1-7. DOI 10.1109/08IAS.2008.356.
2. D. Cvoric, S.W.H. de Haan and J.A. Ferreira, *New Saturable-Core Fault Current Limiter Topology with Reduced Core Size*, Sixth IEEE International Power Electronics and Motion Control Conference (IPEMC) 2009, pp 920–926. DOI 10.1109/IPEMC.2009.5157515.
3. S. Wolfus, A. Friedman, Y. Yeshurun, V. Rozenshtein and Z. Bar-Haim, *Fault Current Limiters (FCL) with the Cores Saturated by Superconducting Coils*, International Application Published Under the Patent Cooperation Treaty, WO 2007/029224 A1, March 2007.
4. F. A. Darmann and F. Darmann: *Superconductor Current Limiting System and Method*, US 2007/0115598 A1, May 2007.
5. J. Jin: *The Finite Element Method in Electromagnetics*, John Wiley & Sons, US, 1993.
6. www.comsol.com
7. H. De Gersem and T. Weiland, *Field-Circuit Coupling for Time-Harmonic Models Discretized by the Finite Integration Technique*, IEEE Trans. on Magn., 40(**2**), pp. 1334-1337, 2004.
8. P. Dular and J. Ghyselinck, *Modeling of 3-D Stranded Inductors with the Magnetic Vector Potential Formulation and Spatially Dependent Turn Voltage of Reduced Support*, IEEE Trans. on Magn., 40(**2**), pp. 1298-1301, 2004.
9. D. Lahaye, S. Vandewalle and K. Hameyer. *An Algebraic Multilevel Preconditioner for Field-Circuit Coupled Problems* IEEE Trans. on Magn., 38(**2**), pp. 413-416, 2002.
10. K. E. Brenan, S. J. Campbell and L. R. Petzold, *Numerical Solution of Initial Value Problems Differential Algebraic Equations* Second Edition, SIAM, 1996.
11. O. Schenk and K. Gärtner, *Two-Level Scheduling in PARDISO: Improved Scalability on Shared Memory Multiprocessing Systems* Parallel Computing, 28, pp. 187-197, 2002.